

Effect of Processing on Inelastic Fracture Behavior of 6061 Aluminum

M.N. Cavalli, T.A. Luoma
Mechanical Engineering Department
University of North Dakota
Grand Forks, ND 58202-8359

ABSTRACT

Statistical concepts from Design of Experiments were used to study the effect of thermal processing on the mechanical properties of 6061 aluminum. The soak temperature, cooling rate and soak temperature/cooling rate interaction term were found to be the most influential processing variables. Soak time and heating rate were statistically insignificant in the current experimental design, but modifications to the experimental method are discussed to study the influence of these factors. Micrographs of specimens subjected to two different processing schemes are presented and discussed. The integration of the results of the work into a general study of the ductile fracture behavior of aluminum alloys is discussed.

INTRODUCTION

Fracture in engineering materials, particularly metals, has been widely studied. The concept of Linear Elastic Fracture Mechanics (LEFM) is a powerful technique for understanding fracture behavior when the amount of plastic deformation prior to fracture is relatively small [1]. Tools such as the crack-tip opening displacement (CTOD) [1] and the J-integral [2] expand our analysis capabilities when significantly more plastic deformation is present prior to fracture. In the presence of massive plastic deformation and ductile fracture, however, even these approaches cannot measure geometry-independent properties [1]. This limitation can lead to severe design restraints or expensive experimental validation procedures in applications such as aerospace and automotive structures where high strength and stiffness with low weight are desired.

As a result, a need exists to be able to understand and predict the ductile fracture behavior of metals. In aerospace and automotive applications, the metal of interest is typically aluminum. Ductile fracture in aluminum is associated with the nucleation, growth and coalescence of voids within the microstructure [1]. One approach that has been used to model this behavior follows an analysis after that of Gurson [3], who considered the growth of spherical voids in a homogenous matrix. Various corrections to the original Gurson model have been proposed to allow for instability and final fracture of the material [4,5]. One of the most promising models is the so-called 'Complete Gurson Model' of Zhang *et al.* which combines a yield function based on the void volume fraction with expressions for calculating void nucleation and growth as well as plastic instability in material between adjacent voids [6]. This model was implemented into the finite element code ABAQUS and showed good agreement with strength measurements in two weld geometries [7]. Zhang *et al.* have also developed a method to link some of the model parameters from the Complete Gurson Model to the processing history of the material using the program WELDSIM and a specialized mapping algorithm [7].

Results of the study of Zhang *et al.* showed that strength predictions from the Complete Gurson Model were in good agreement with experimental results if slight adjustments were made to the void nucleation parameters for each test geometry [7]. A direct, geometry-independent link between the void nucleation parameters and the processing history is not yet available [7]. To explore the link between strength and microstructure, Myhr *et al.* have constructed a thermodynamic framework to predict strengthening and hardness based on particle evolution [8]. While the results are encouraging, a fully coupled, predictive processing/fracture model does not yet exist. As a result, the full potential of numerical modeling techniques to reduce the required number of experiments for validation of design performance cannot be completely realized.

The current work is part of a larger project to provide a statistical link between material processing and ductile fracture behavior of aluminum alloys. Fracture experiments, microstructural analyses and numerical calculations will be combined to allow the fracture behavior of aluminum alloys to be predicted based solely on knowledge of their thermal and mechanical processing history. The final goal of the overall project is to link every parameter in the Complete Gurson Model to measurable processing variables. This paper presents experimental results and statistical analyses from tests on 6061 aluminum samples that were subjected to a variety of heating and cooling sequences.

EXPERIMENTAL METHOD

Standard dogbone tensile specimens were machined from 6061-T6 sheet stock (0.1875 in. thickness) in accordance with ASTM Standard E8 [9]. To remove any effects of work hardening on the results, these specimens were annealed at 775 °F for

two hours. After two hours, the specimens were cooled at a rate of 50 °F/hour until 500 °F and then the oven was turned off and the specimens were allowed to cool room temperature. It is expected that this treatment will have removed the effects of the original T6 condition [10]. Each sample was then subjected to a heat treatment following the schematic of Figure 1.

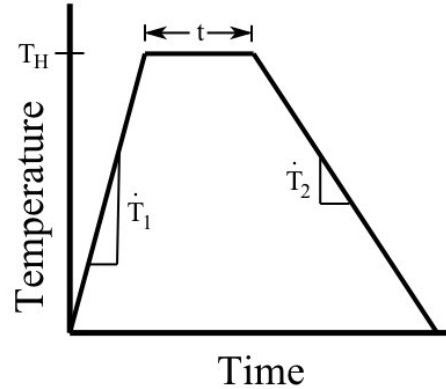


Figure 1: Heat treatment history of the experimental samples.

Statistics based on Design of Experiments (DOE) concepts [11] were used to assign random values of the processing parameters shown in Figure 1 to each of the experimental specimens. The heating rate, \dot{T}_1 , was varied by placing the specimens in a preheated furnace (+) or a room temperature furnace (-), the soak temperature (T_H) was either 788 °F (-) or 1022 °F (+), the holding time (t) was either 60 minutes (-) or 2.5 hours (+) and the cooling rate, \dot{T}_2 , was either furnace cooled (-) or water quenched (+) for each specimen. For a four variable system, a full factorial setup consists of $2^4 = 16$ test specimens. An appropriate randomized test matrix can be found in the reference [11]. Immediately following heat treatment, each specimen was placed in a refrigerator at 38 °F. After all specimens were heat-treated, all specimens were removed from the refrigerator and allowed to age at room temperature for four days and four hours. The samples were then returned to the refrigerator for approximately two weeks until testing.

Each sample was tested under displacement control in a hydraulic testing machine (Tinius-Olsen, Super “L” Universal Testing Machine). Load and strain information were provided by the machine load cell and an attached extensometer, respectively. Additional strain data was captured using a 2D digital image correlation system (Correlated Solutions). Good agreement was found between both sources of strain data. Following testing the specimens were placed back into the refrigerator for storage prior to microstructural examination.

From the testing data, a true stress-strain curve for each specimen was constructed. Yield stress, fracture stress, fracture strain, and the area under the true stress-strain curve were all calculated. Finally, the plastic portion of the stress-strain curve was fitted using the relationship [12]

$$\bar{\sigma} = \sigma_Y + K\bar{\epsilon}^n \tag{1}$$

where $\bar{\sigma}$ is the equivalent stress, $\bar{\epsilon}$ is the equivalent plastic strain, σ_Y is the yield stress, and K and n are material constants.

After testing, a portion of the unstressed gripping region of each specimen was sectioned and polished for microstructural examination. Full data on inclusion size and shape have not yet been compiled, but representative micrographs will be presented.

EXPERIMENTAL RESULTS

Experimental results from the tension tests tended to cluster near either a low strength, high elongation result or a high strength, low elongation result. Some distribution between these limits was seen, but most samples tended to exhibit behavior similar to one of the curves shown in Figure 2. The specific curves shown in Figure 2 represent the highest and lowest strength results obtained from the experimental runs.

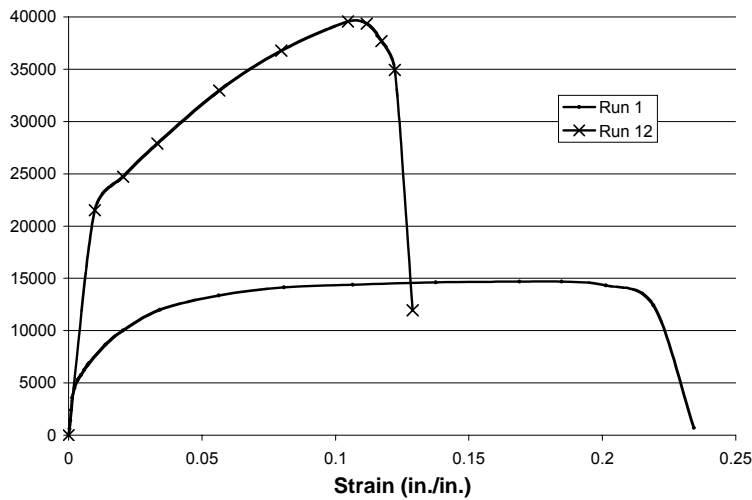


Figure 2: Stress-strain results from two experimental specimens representing the bounds of the material data

Table 1 shows the values of the four processing variables that correspond to runs 1 and 12. Perhaps not surprisingly, the low strength, high elongation behavior (run 1) corresponds to a low processing temperature and a slow cooling rate. In contrast, the high strength specimen (run 12) was subjected to a high temperature and fast quench.

Table 1: Processing variable values for samples shown in Figure 2

Run	\bar{T}_1	T_H ($^{\circ}F$)	t (hours)	\bar{T}_2
1	Cold Furnace	788	1	Furnace Cooled
12	Preheated Furnace	1022	2.5	Water Quenched

Figures 3 and 4 show optical micrographs of an annealed sample (similar in processing history to run 1) and of sample 12, respectively. Noticeable differences in the microstructure of the two specimens are evident. Specifically, many of the particles in the annealed image are much larger and have higher aspect ratios than those found in the quenched sample. The dispersed array of fine particles in Figure 4 leads to both a stronger and tougher material.

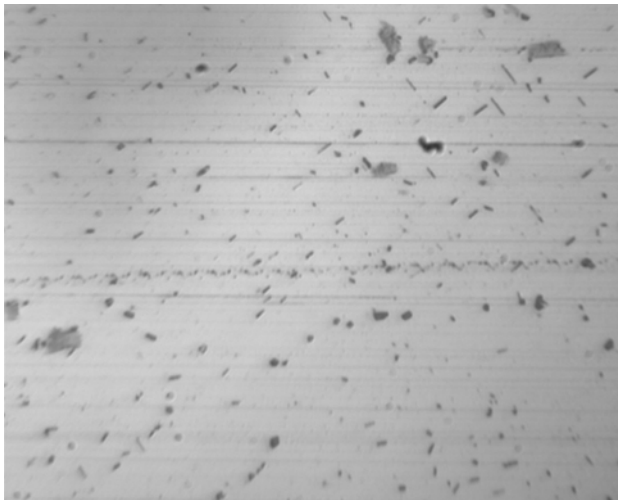


Figure 3: Micrograph of annealed specimen at 1500X magnification



Figure 4: Micrograph of specimen 12 at 1500X magnification

STATISTICAL ANALYSIS

Statistical analyses were conducted on the experimental results to determine the relationships between σ_f , σ_y , ϵ_f , A , n , and the area under the true stress-strain curve and the processing history of the material. The analysis is performed according to DOE concepts. Using the Student's t Statistic, a threshold is defined that determines the significance of the effect of each of the four variables on the material behavior, as well as the effect of all two-variable interaction terms [11]. It was determined that

the only test parameters with statistically significant influence on material properties were the soak temperature, T_H , the cooling rate, \dot{T}_2 , and the interaction term, $T_H\dot{T}_2$. Mathematically,

$$\Omega = f(T_H, \dot{T}_2, T_H\dot{T}_2) = C_1 + C_2\alpha + C_3\beta + C_4\alpha\beta \quad (2a)$$

$$\alpha = \left(\frac{T_H - 905}{117} \right) = \begin{cases} -1 \rightarrow T_H = 788^\circ \text{F} \\ 1 \rightarrow T_H = 1022^\circ \text{F} \end{cases} \quad (2b)$$

$$\beta = \dot{T}_2 = \begin{cases} -1 \rightarrow \text{furnace cooled} \\ 1 \rightarrow \text{water quenched} \end{cases} \quad (2c)$$

where Ω is the property of interest, $C_1 - C_4$ are constants, and the units of T_H are $^\circ\text{F}$. Values of the constants for each material property are tabulated in Table 2.

Table 2: Statistical constants for processing effects on material properties

Property	C_1	C_2	C_3	C_4
σ_f	23300	4900	5400	4700
σ_y	8850	3420	3380	3030
ϵ_f	0.179	-0.0285	-0.0165	0
A	40100	12900	13200	11900
n	0.23	0.025	0.028	0.026
Area	3180	0	312	343

It should be noted that this analysis is based solely on endpoints for each of the variables (*i.e.* a linear analysis). One expects some amount of curvature in the solution space for these variables. These effects are currently being explored. In addition, the uncertainty in each of the constants was estimated from the accuracy of the respective experimental measurements. A full analysis of the actual uncertainty following the statistical analysis has not yet been performed.

DISCUSSION

From Table 2, we see that, within the respective equations for four of the material properties, the values of C_2 , C_3 , and C_4 are approximately equal. Using the true ultimate strength as an example, the equation resulting from the statistical analysis is:

$$\sigma_f = 23000 + 4900\alpha + 5400\beta + 4700\alpha\beta \quad (3)$$

A value of $\alpha = -1$ corresponds to a heat-treatment at the lower temperature bound, 788°F . Regardless of the cooling rate, Equation 3 predicts that the ultimate strength corresponding to this heat-treatment will be near the lower curve shown in Figure 2. This makes sense phenomenologically because the lower soak temperature is beneath the solvus temperature limit for 6061 Al ($\sim 959^\circ\text{F}$) as shown in Figure 5. As a result, no solution strengthening is achieved even if the material is quenched from this temperature.

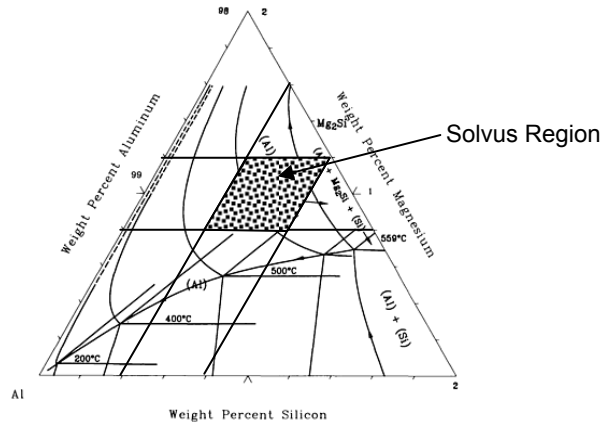


Figure 5: Ternary phase diagram for Al-Si-Mg [13] with solvus region for 6061 aluminum (0.4-0.8% Si, 0.8-1.2% Mg [9])

Based on the concept of the solvus temperature, one might expect a very obvious change in material behavior near a certain narrow temperature band, assuming uniform distribution of the solute elements. Due to the choice of upper and lower temperature bounds in this work (with the lower bound at the start of the annealing range and the upper bound at the top of the solutionizing range), the sudden change to solution heat-treating is not captured. Additional specimens with soak temperatures between the bounding data might be able to quantify the effects. This concept helps explain the fact that neither the heating rate, \dot{T}_1 , nor the soak time, t , were found to be statistically significant. Since the specimens were annealed prior to testing, heating them to the annealing temperature again should have no effect, regardless of the time. In contrast, heating the specimens to the solutionizing temperature for a specific amount of time should have some effect on the results if the time at temperature is sufficient for at least some of the alloying elements to go into solution. However, as only a portion of the experimental samples are processed at high temperature, the effects of both time and heating rate would have to be very large to show up as statistically significant to the entire experimental group.

To study the transition from annealing heat-treating to solution heat-treating, more meaningful results might be obtained by splitting the temperature range into two parts, one centered in the annealing range ($\sim 700^\circ\text{F}$) and the other centered in the solutionizing range ($\sim 1000^\circ\text{F}$) [10]. Similarly, it might be advisable to have the samples in some state of both prior thermal treatment and prior strain hardening, rather than the annealed condition, at the start of the heat-treating process. Changes in the material properties could then be expected to occur regardless of which temperature range is used. Both of these changes to the experimental protocol are currently being implemented.

The statistical equations for two material properties are different from the others in that not all three variables in Equation 2 are statistically significant. The soaking temperature is significantly more important on the failure strain than the cooling rate and the interaction term has negligible impact. Both the cooling rate and the interaction term affect the area under the curve but the soaking temperature does not.

$$\varepsilon_f = 0.179 - 0.0285\alpha - 0.0165\beta \quad (4a)$$

$$Area = 3180 + 312\beta + 343\alpha\beta \quad (4b)$$

The largest fracture strains are achieved in specimens that are treated at the lowest temperature ($\alpha = -1$) and are furnace cooled ($\beta = -1$). These specimens do not, however, demonstrate the largest value of area under the curve. Maximum values of area under the curve (related to the toughness of the material) are achieved for fast cooling times ($\beta = 1$) and high soaking temperatures. These results indicate that both strength and toughness are improved through solution heat-treating. In other words, the increase in strength due to solution heat-treating more than offsets the reduction in fracture strain for a net gain in area under the curve (Figure 2). As the aging time and temperature were not included as variables, aging effects on the material properties cannot be quantified separately.

CONCLUSIONS

This work has outlined the general application of concepts from Design of Experiments to the thermal processing of aluminum alloys. Work is currently underway to refine the process to more clearly elucidate the material behavior/processing interaction by including both thermal and mechanical pretreatments as well two distinct soak temperature ranges. A complete analysis of the uncertainty in the fitting parameters is needed to give an accurate picture of the applicability of the results. In addition, quantitative links between the measured material properties and observed microstructural features (inclusions and second phase particles) still need to be developed. Future work will include additional test geometries and numerical fracture simulations to give a complete ductile fracture model based on thermal and mechanical processing history.

ACKNOWLEDGEMENTS

The authors would like to thank ND EPSCoR, the UND School of Engineering and Mines and the Department of Mechanical Engineering for equipment funding and support of Mr. Luoma during the course of this project.

REFERENCES

1. Anderson, T.L., *Fracture Mechanics: Fundamentals and Applications*, CRC Press, New York, 1995.
2. Rice, J.R., "A Path Independent Integral and the Approximate Analysis of Strain Concentration by Notches and Cracks," *Journal of Applied Mechanics*, **35**, 379-386.
3. Gurson, A.L., "Continuum Theory of Ductile Rupture by Void Nucleation and Growth: Part I—Yield Criteria and Flow Rules for Porous Ductile Media," *Journal of Engineering Materials and Technology*, 2-13, 1977.
4. Tvergaard, V., "On Localization in Ductile Materials Containing Spherical Voids," *International Journal of Fracture*, **18**, 237-252, 1982.
5. Thomason, P.F., "A Three-Dimensional Model for Ductile Fracture by the Growth and Coalescence of Voids," *Acta Metallurgica*, **33**, 1087-1095, 1987.

6. Zhang, Z.L., C. Thaulow, J. Odegard, "A Complete Gurson Model Approach for Ductile Fracture," *Engineering Fracture Mechanics*, **67**, 155-168, 2000.
7. Zhang, Z.L., J. Odegard, O.R. Myhr, H. Fjaer, "From Microstructure to Deformation and Fracture Behaviour of Aluminum Welded Joints – A Holistic Modelling Approach," *Computational Materials Science*, **21**, 429-435, 2001.
8. Myhr, O.R., O. Grong, H.G. Fjaer, C.D. Marioara, "Modelling of the Microstructure and Strength Evolution in Al-Mg-Si Alloys During Multistage Thermal Processing," *Acta Materialia*, **52**, 4997-5008, 2004.
9. Standard E8, "Standard Test Method for Metallic Materials," American Society for Testing and Materials, West Conshohocken, PA, 1998.
10. Standard B597, "Standard Practice for Heat Treatment of Aluminum Alloys," American Society for Testing and Materials, West Conshohocken, PA, 1998.
11. Lawson, J., J. Erjavec, Modern Statistics for Engineering and Quality Improvement, Thomson-Duxbury, Singapore, 2001.
12. Holloman, J.H., *Transactions of AIME*, **162**, pp. 268, 1945.
13. Willey, L.A., Metallography, Structures and Phase Diagrams, Vol 8, Metals Handbook, 8th ed., American Society for Metals, Metals Park, OH 1973.